# SUPPORTING INFORMATION

## Rapid Millifluidic Synthesis of Stable High Magnetic Moment $Fe_xC_y$ Nanoparticles for Hyperthermia

*Katerina Loizou*[a], *Stefanos Mourdikoudis*[b,c], *Andreas Sergides*[b,c], *Maximilian O. Besenhard*[a], *Charalampos Sarafidis*[d], *Koichi Higashimine*[e], *Orestis Kalogirou*[d], *Shinya Maenosono*[e], *Nguyen Thi Kim Thanh*[b,c,*], *Asterios Gavriilidis*[a,*]

[a] Department of Chemical Engineering, University College London, Torrington Place, London, WC1E 7JE, UK

[b] Biophysics Group, Department of Physics and Astronomy, University College London, Gower Street, London, WC1E 6BT, UK

[c] UCL Healthcare Biomagnetic and Nanomaterials Laboratories, 21 Albemarle Street, London, W1S 4BS, UK

[d] Department of Physics, Aristotle University of Thessaloniki, 54124, Thessaloniki, Greece

[e] School of Materials Science, Japan Advanced Institute of Science and Technology, 1-1 Asahidai, Nomi, Ishikawa 923-1292, Japan

* e-mail: ntk.thanh@ucl.ac.uk, a.gavriilidis@ucl.ac.uk

**Contents**

## S1. TEM images of the synthesized nanoparticles

Following up from Figure 2 in the main manuscript, where the effect of temperature on the size and dispersity of the synthesized nanoparticles is presented, TEM images for samples prepared at temperatures between 200 $^{o}$C and 240 $^{o}$C are shown in Figure S1.

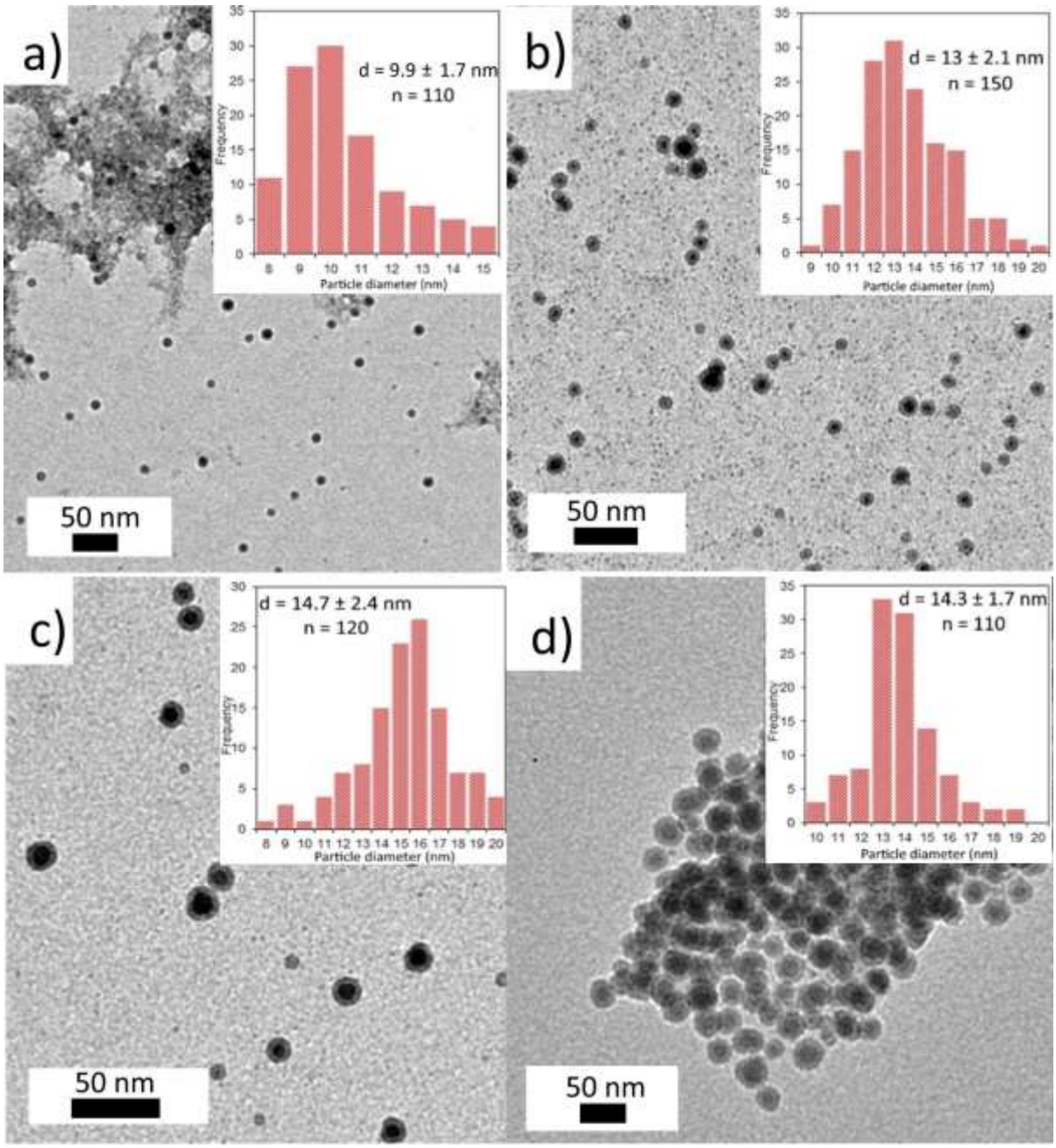


**Figure S1.** TEM images of nanoparticles synthesized at a) 200 °C, b) 215 °C, c) 230 °C, d) 240 °C. d is the diameter of the nanoparticles measured from the TEM images, n is the number of nanoparticles measured for each histogram.

## S2. Yield and productivity of the millifluidic synthesis

Table S1 shows the nanoparticle productivity and yield of the continuous flow reactor. The yield is calculated by:

$$Yield\ \% = \frac{Nanoparticle\ productivity\ (\frac{mg_{Fe}}{h})}{Inlet\ mass\ flow\ rate\ (\frac{mg_{Fe}}{h})} \times 100\ \%$$

The nanoparticle productivity is calculated based on the MP-AES elemental analysis (for Fe) performed for each sample, taking into account the outlet mass flow rate. The inlet mass flow rate for Fe is calculated based on the total amount of iron which enters the system (in the form of iron pentacarbonyl).

**Table S1:** Nanoparticle productivity and yield (%) for the millifluidic synthesis of $Fe_xC_y$ NPs.

| Reaction temperature (°C) | Nanoparticle productivity ($mg_{Fe}$/min) | Yield % |
|---|---|---|
| 230 | 0.19 | 14.6 |
| 240 | 0.29 | 22.2 |
| 250 | 0.38 | 28.8 |
| 265 | 0.50 | 38.1 |

## S3. XRD measurements of the synthesized nanoparticles and reference patterns

In Figure S2 the raw data (without deconvolution) are shown for three samples synthesized at different temperatures in the flow reactor. The samples were analyzed a few hours after the synthesis and washing stages. Focusing at the two samples synthesized at the two higher temperatures (230 $^{o}$C and 265 $^{o}$C), Rietveld refinement of the XRD patterns was performed using the FullPROF software, as explained in the main manuscript. The Rietveld analysis generates simulated reference patterns which are shown in Figure S3 below. The reference patterns (Figure S4-S7) of hematite, α-Fe, magnetite and $Fe_5C_2$ were taken from the PANalytical X'Pert HighScore Plus software.

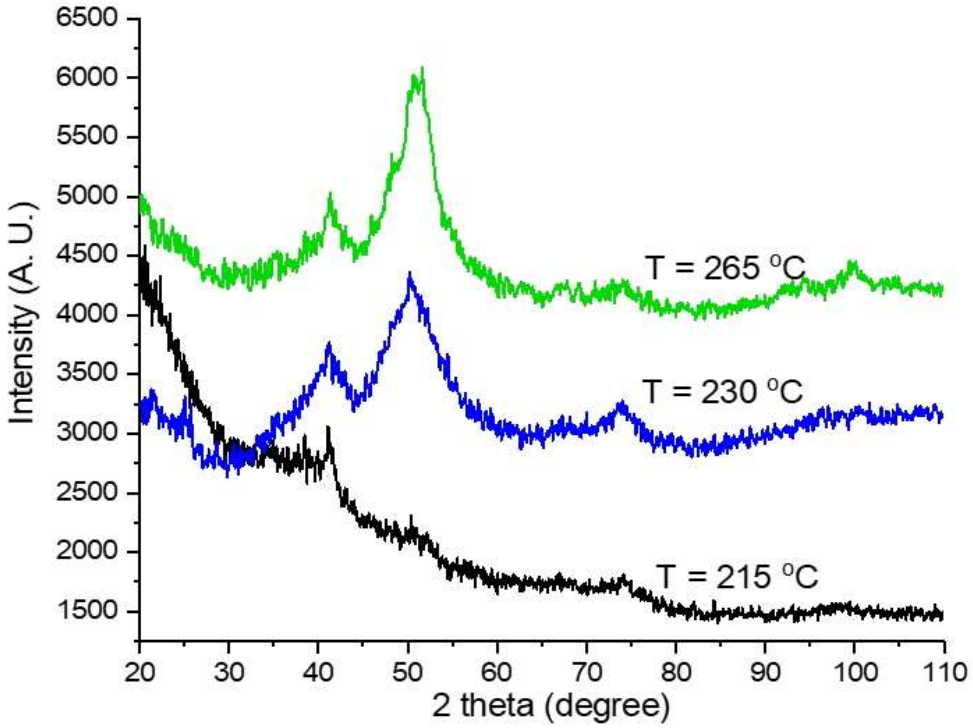


**Figure S2.** Powder XRD patterns of samples synthesized by flow synthesis at various temperatures.

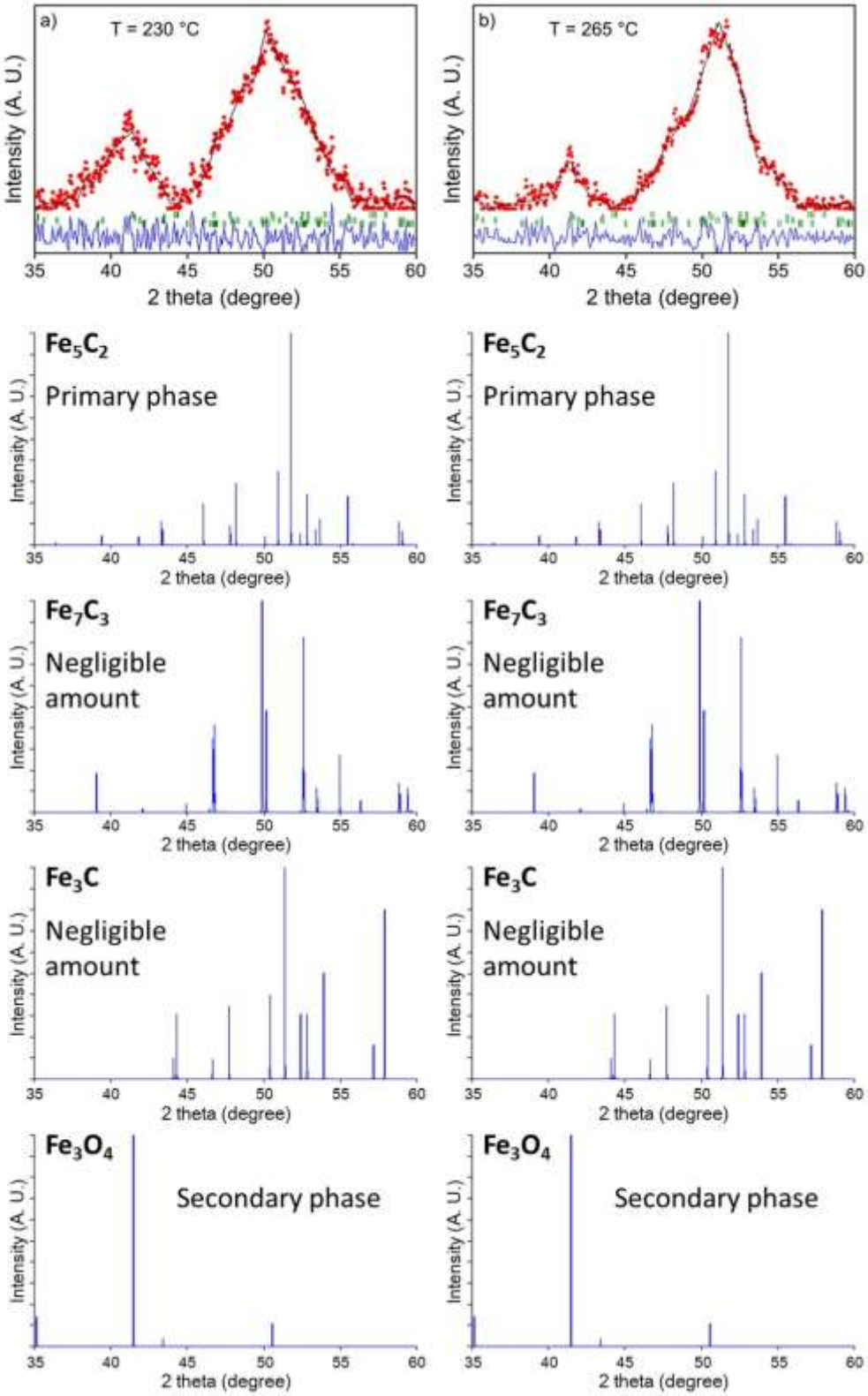


**Figure S3.** Powder XRD patterns of nanoparticles synthesized in flow at a) 230 ºC and b) 265 ºC, together with the peak positions of the simulated reference patterns of their component materials.

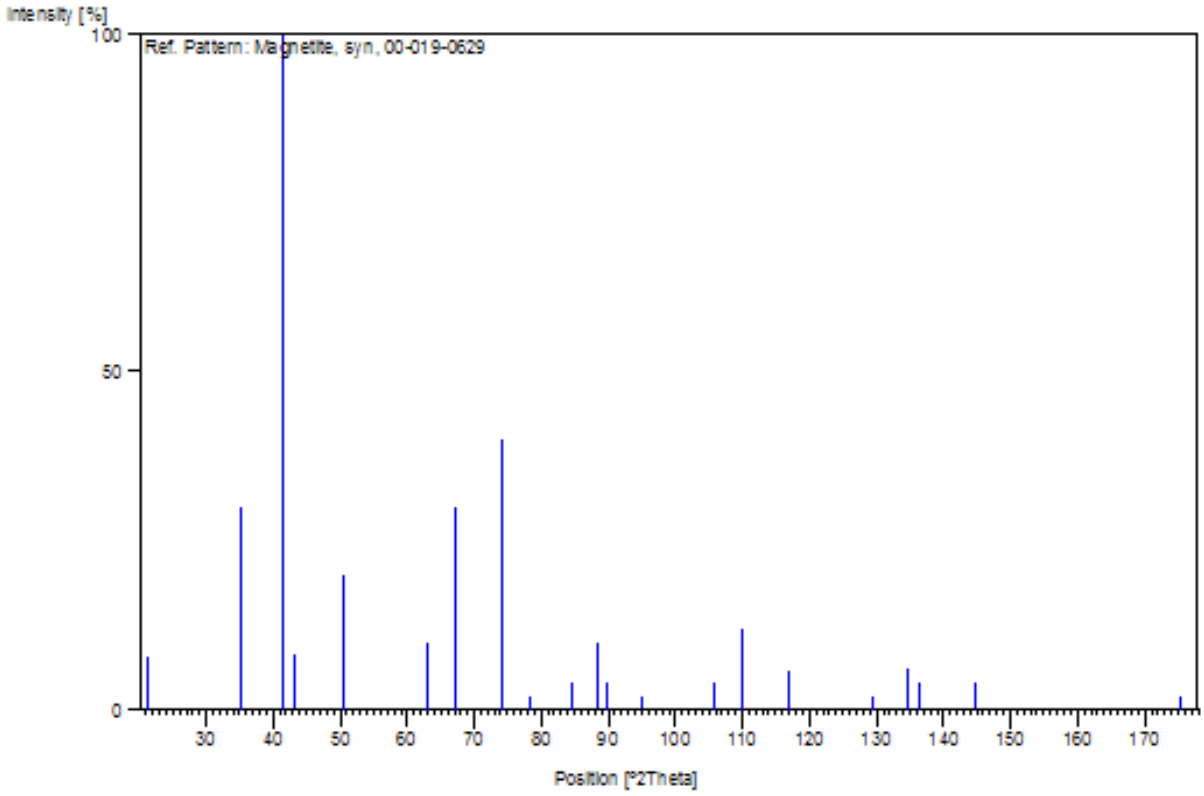


**Figure S4.** Reference pattern for magnetite ($Fe_3O_4$), reference code: 00-019-0629.

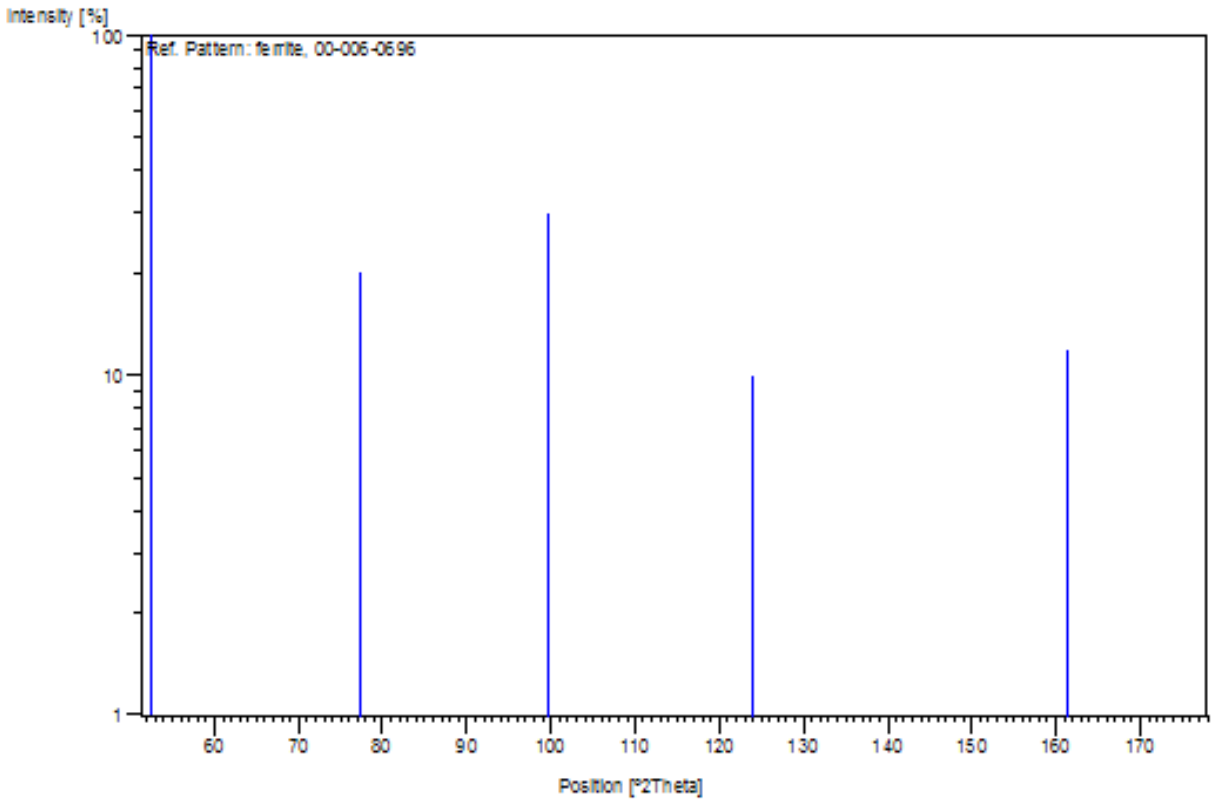


**Figure S5.** Reference pattern for α-Fe (reference code: 00-006-0696).

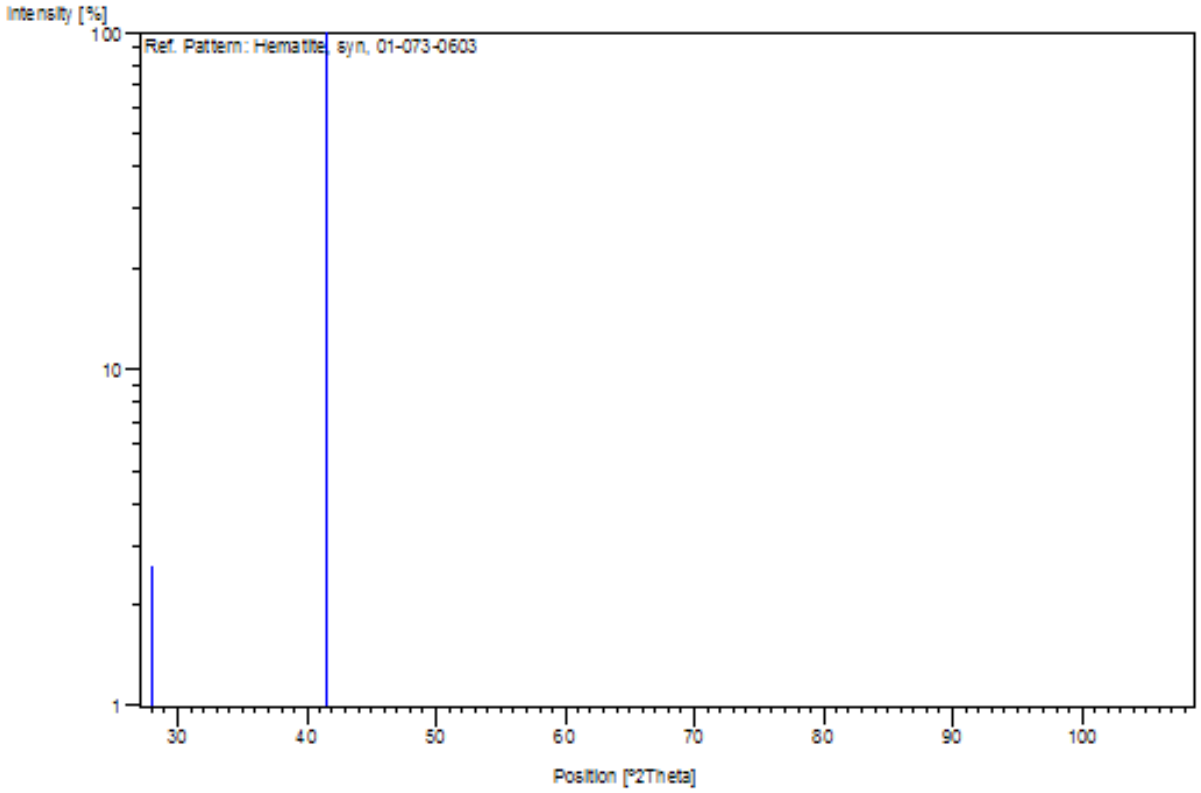


**Figure S6.** Reference pattern for hematite ($\alpha$-$Fe_2O_3$), reference code: 01-073-0603.

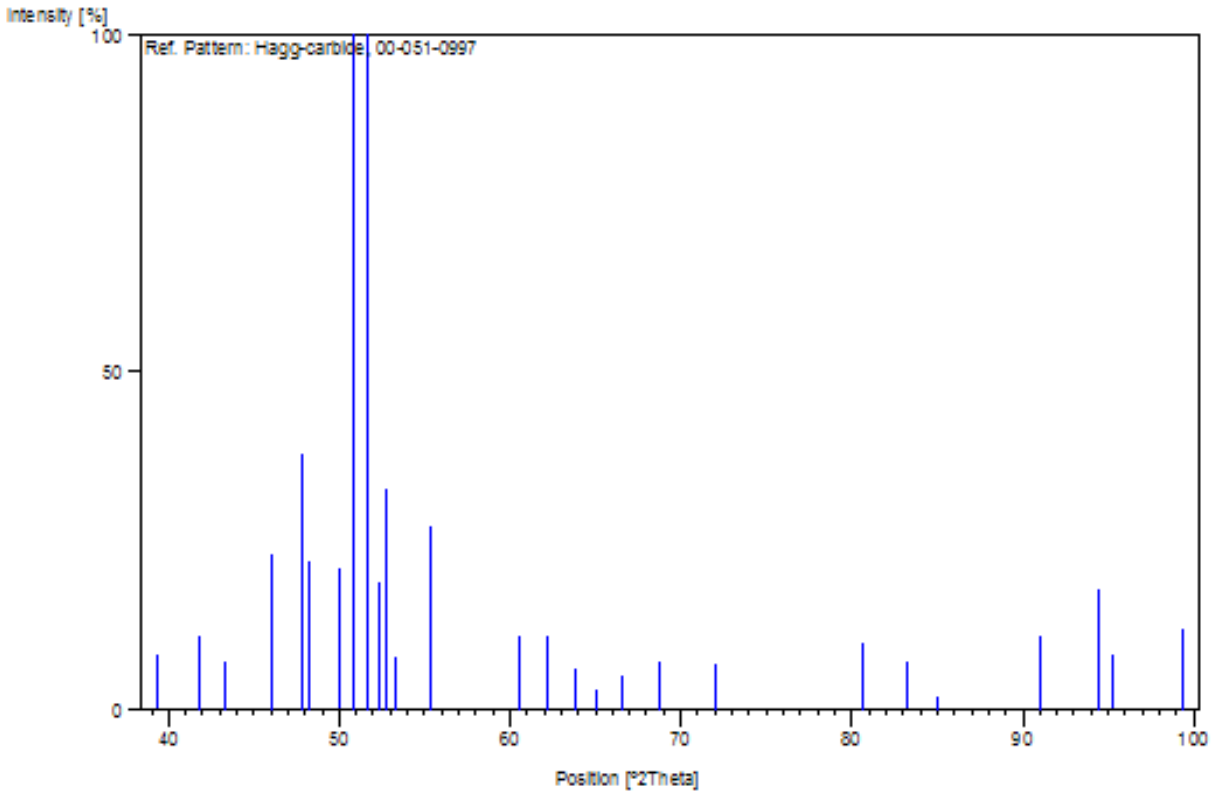


**Figure S7.** Reference pattern for iron carbide ($Fe_5C_2$), reference code: 00-051-0997.

## S4. HRTEM-HAADF-STEM-EDS measurements of the NPs synthesized at 230 ºC

Apart from the sample synthesized at 265 ºC, the sample synthesized at 230 ºC was also analysed by HRTEM-HAADF-STEM-EDS techniques. The core-shell structure and the distribution of the different elements throughout the particle volume are observed in Figure S8.

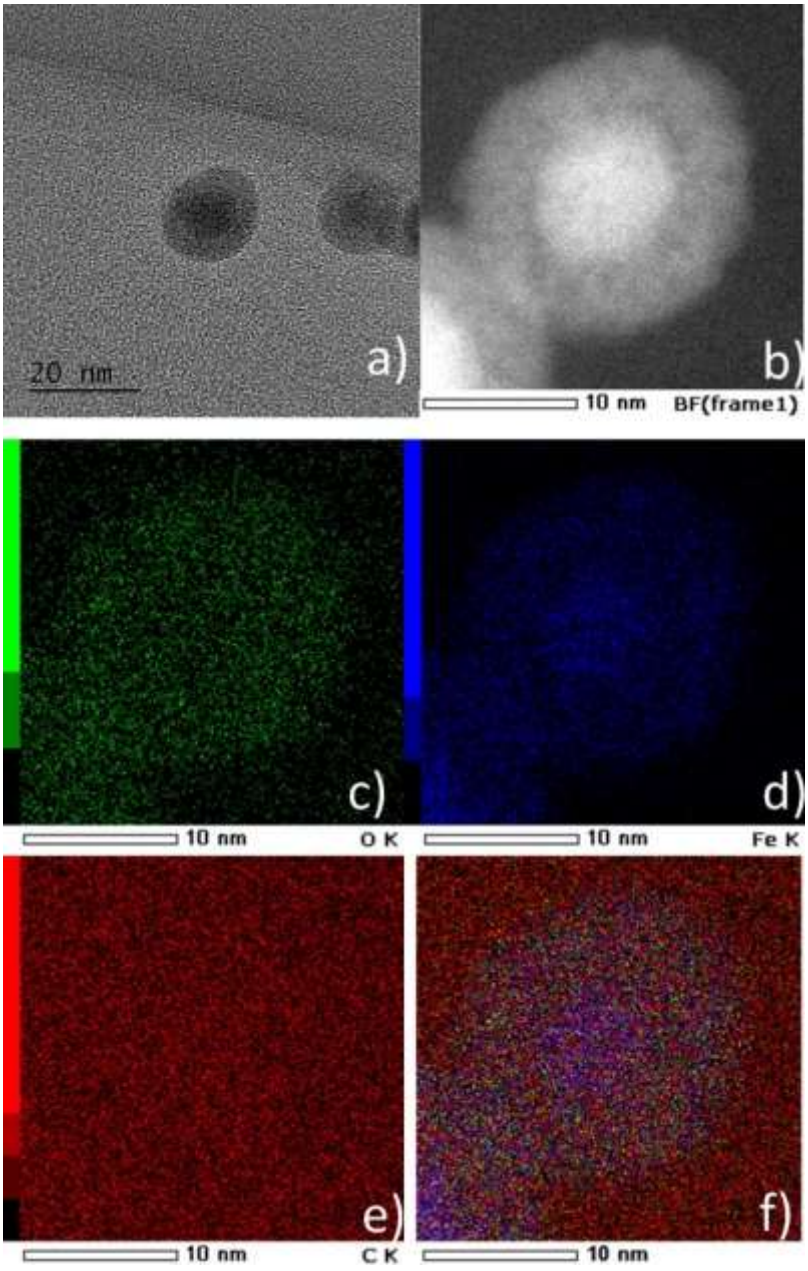


**Figure S8.** a) HRTEM image, b) HAADF-STEM bright field image, and corresponding EDS elemental mapping images: c) O K edge, d) Fe K edge, e) C K edge, and f) overlay, for nanoparticles synthesized at 230 ºC.

## S5. Solubility data for carbon monoxide

Since there are no data on the solubility of CO in 1-octadecene in the literature, its solubility was compared to that in 1-octene and hexadecane, as shown below. Figure S9 supports that the solubility of CO at the lower CO partial pressures encountered in batch systems is significantly smaller than at higher partial pressures, assuming that CO is the only gas present. Therefore, it is postulated that in our millifluidic system the increased amount of CO present enhances the carbidization at lower temperature, acting as an additional carbon source (apart from oleylamine).

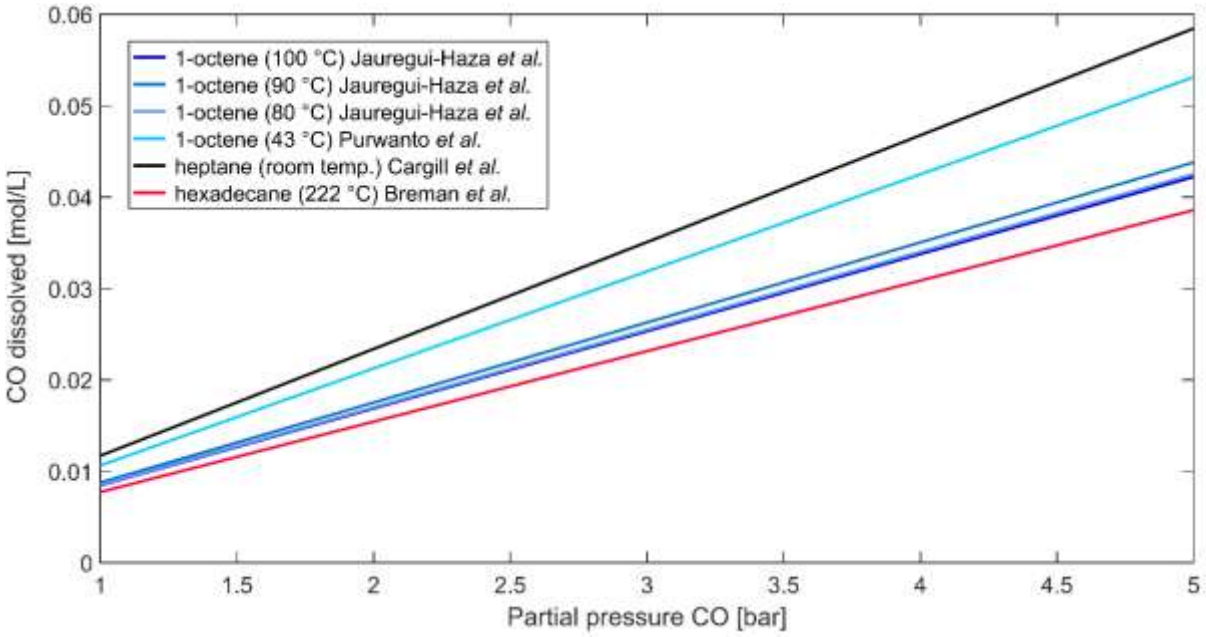


**Figure S9.** Solubility of CO in different organic solvents plotted as a function of the partial pressure of CO at the indicated temperature for each dataset. Data were obtained from Jauregui-Haza *et al.* (3).

## S6. Hyperthermia measurements of nanoparticles synthesized in batch

The samples synthesized at 250 ºC by both methods (batch and flow) showed similar heating efficiencies. Concerning the samples synthesized at the highest temperatures (280 ºC for batch, 265 ºC for flow), the batch sample had considerably smaller ILP value (see Table S2), in comparison to the flow sample (Table 3 at manuscript). It seems that for the highest synthesis temperatures, a combination of bigger particle size (see Figure 4 at the manuscript) and probably a higher degree of carbidization for the flow-prepared sample resulted in a substantial increase of its heating ability.

**Table S2:** Specific absorption rate and intrinsic loss power values for the nanoparticles synthesized at different temperatures via batch synthesis.*

| Reaction Temperature (°C) | Specific Absorption Rate, SAR (W $g^{-1}$) | Intrinsic Loss Power, ILP (nH $m^2$ $kg^{-1}$) |
|---|---|---|
| 250 | 30.7 | 0.1 |
| 280 | 99.6 | 0.34 |

**These measurements were performed with a frequency of 488 kHz.*

## References

(1) Breman, B. B.; Beenackers, A. A. C. M.; Rietjens, E. W. J.; Stege, R. J. H. Gas-liquid solubilities of carbon monoxide, carbon dioxide, hydrogen, water, l-alcohols ($l \leq n \leq 6$), and n-paraffins ($2 \leq n \leq 6$) in hexadecane, octacosane, 1-hexadecanol, phenanthrene, and tetraethylene glycol at pressures up to 5.5 MPa and temperatures from 293 to 553 K. *J. Chem. Eng. Data*, **1994**, 39, 647-666.

(2) Cargill, R.W. Solubility Data Series. Pergamón Press: New York**, 1990**, 51-52.

(3) Jáuregui-Haza, U. J.; Pardillo-Fontdevila, E. J.; Wilhelm, A. M.; Delmas, H. Solubility of hydrogen and carbon monoxide in water and some organic solvents. *Lat. Am. Appl. Res.*, **2004**, 34, 71-74.

(4) Purwanto, Deshpande, R. M.; Chaudhari, R. V.; Delmas, H. Solubility of hydrogen, carbon monoxide, and 1-octene in various solvents and solvent mixtures. *J. Chem. Eng. Data*, **1996**, 41, 1414-1417.